In Vivo Live Imaging of Bone Using Shortwave Infrared Fluorescence Quantum Dots

Yanjun Che
First Affiliated Hospital of Soochow University
Sijia Feng
Huashan Hospital Fudan University Department of Sports Medicine
Jiangbo Guo
First Affiliated Hospital of Soochow University
Junjun Hou
Department of Geriatrics, Xinghu Hospital, Suzhou, Jiangsu
Xuesong Zhu
First Affiliated Hospital of Soochow University
Liang Chen
First Affiliated Hospital of Soochow University
Huilin Yang
First Affiliated Hospital of Soochow University
Mo Chen
Huashan Hospital Fudan University Department of Sports Medicine
Yunxia Li
Huashan Hospital Fudan University Department of Sports Medicine
Shiyi Chen
Huashan Hospital Fudan University Department of Sports Medicine
Zhen Cheng
Department of Radiology, Stanford University
Zongping Luo
First Affiliated Hospital of Soochow University
Jun Chen (biochenjun@fudan.edu.cn)
Huashan Hospital Fudan University Department of Sports Medicine

---

Short Communication

Keywords: bone, in vivo imaging, bioimaging, Shortwave Infrared, live imaging

Posted Date: August 27th, 2020

DOI: https://doi.org/10.21203/rs.3.rs-65440/v1

Version of Record: A version of this preprint was published at Nanoscale on January 1st, 2020. See the published version at https://doi.org/10.1039/D0NR06261H.

Abstract

Bone is playing an increasingly critical role in human health and disease. More noninvasive multi-scale imaging techniques are urgently required for investigations on the substructures and biological functions of bones. Our results firstly revealed that our prepared SWIR QDs acted as a bone-specific image contrast to achieve real-time imaging of bone structures both *in vivo* and *ex vivo*. The major bone structures of both Balb/C nude mouse and Balb/C mouse including the skull, spine, pelvis, limbs and the sternum could be rapidly and gradually identified via blood circulation after QDs injection *in vivo*. More importantly, the binding capability of our QDs mainly depend on the biological activities of bone tissues, suggesting our technique was suitable for *in vivo* live imaging. Additionally, the cell imaging results suggested that the potential mechanism of our bone imaging could be ascribed to the highly specific interaction between QDs and MC3T3-E1 cells. In a word, skeletal structures and biological activities of bones are anticipated to be observed and monitored with this QDs-guided SWIR imaging strategy, respectively. This radiation-free QDs-guided SWIR live imaging of bone can put new insights into a comprehensive study of bones *in vivo* and provide basis for early diagnosis of bone diseases.

Introduction

As one of the basic organs in our body, bone is not only a fundamental mechanical structural unite for body motion, but also acts as a metabolic storage for minerals, stem cells and biological factors needed for life functions[1–3]. Both injury and disease of bones can lead to significant morbidity including osteoporosis, loss of mobility, metabolic derangements and disability, etc. Thus, it is essential to comprehensively understand the role of bones human health and disease.

Nowadays, identification of bone structures is mainly dependent on imaging techniques. As is known to all, X-ray-based imaging including computed tomography (CT) have long been widely applied for investigating bone structures for almost one century in clinic. However, owing to radiation and low resolution (at ~ mm level), X-ray imaging is considered not suitable for a long-time study of bone tissues from an organ level to a molecular level[4, 5]. Therefore, it is in urgent need to develop a multi-scale imaging approach to visualize the morphology of bones on microscale, even nanoscale.

Optical imaging is currently treated as a promising imaging modality for bone imaging due to its high spatiotemporal resolution, high imaging speed and zero radiation. It has been reported that light-sheet fluorescence imaging can facilitate investigation on bone structures at a cellular level *in vitro*[6, 7], even at a nanoscale level for single molecular fluorescence imaging *in vitro*[8, 9]. However, the intrinsically limited tissue penetration depth of this traditional fluorescence imaging against the high-density cortical bone layer has hindered its further applications for *in vivo* bone imaging.

Fortunately, fluorescence imaging at the shortwave infrared window (SWIR, 1000–1700 nm) is emerging as a powerful *in vivo* imaging tool for biomedical applications[10–16]. As SWIR light is capable of penetrating deeper inner tissues with lower diffusion and refraction in comparison with visible and near-

infrared light (400–900 nm)[17–19]. More recently, SWIR imaging, as an image-guided surgery system, has been successfully applied in clinical practice[20], suggesting its tremendous potential and advantages in biomedical imaging in future. Therefore, bone image contrast is the last piece of the puzzle for accomplishing the *in vivo* imaging of bone. To our knowledge, no bone specific imaging contrast has been successfully developed for *in vivo* live imaging to date, as previous bone targeting molecules failed to penetrate the hard cortical bone shell *in vivo*.

Here, as shown in Scheme.1, we presented a highly bone-specific and biocompatible lead sulfide quantum dots (PbS QDs) encapsulated by ribonuclease A (RNase A) with SWIR emission to identify and analyze the morphology and activities of the skeletal system both *in vivo* and *ex vivo* in a real-time and long-time manner. Firstly, a biocompatible SWIR RNase A-PbS QDs was prepared and characterized based on previous method[21]. Then, a real-time and long-time imaging of various bone structures was achieved after QDs injection. During the *in vivo* observation, bone structures were imaged in a 3D configuration with demonstration of bioactivities and high resolution. Furthermore, specific binding between QDs and MC3T3-E1 cells was observed in subsequent *in vitro* experiments. Finally, the biocompatible QDs was entirely cleared out of the body without obvious toxic effects on bone tissues as well as major organs. Our work demonstrated a novel radiation-free *in vivo* imaging approach for real-time and long-term observation of the skeletal system, which would help us to monitor the progress and prognosis of bone disease in future.

Results And Discussion

In this work, RNase A-PbS QDs as a specific bone image contrast was firstly injected through the tail vein of the Balb/C nude mouse to achieve imaging of bone structures. As shown in Movie S1 and S2 in Supporting Information, as the QDs spreads throughout the whole body of the mouse via blood circulation, specific structures of the skeletal system were imaged by detecting the fluorescence signals from the QDs. Moreover, it is noteworthy that multiple structures of the skeletal system could be clearly identified and distinguished from either a posterior (prone position) or anterior (supine position) view. Thus, characteristics of both the posterior and anterior view of the Balb/C nude mouse after QDs injection were fully evaluated through SWIR *in vivo* imaging movies in a real-time manner.

Figure 1a-h was the posterior view of the mouse. After 15 min post-injection, fluorescence signals were firstly detected from the liver, spleen and heart of the Balb/C nude mouse (Fig. 1b and 1c). Then, as shown in Fig. 1d-g, a variety of bone structures gradually started to be observed since 30 min post-injection. Specifically, from axial bones (the parietal bone, maxilla, spine, pelvis) to limb bones (the humerus, radius and ulna, metacarpus, femur, tibiofibula, calcaneus, phalanges), from upper to lower extremities, from proximal to distal bones as well as major joints (the elbow, wrist, hip, knee, ankle), morphology of bone structures all above were identified in a fixed order with labelling by SWIR fluorescence. During the longitudinal observation, the fluorescence intensity (FL) measured from specific bone structures reached a peak around 1 h post-injection, and then slowly faded with increasing observation time (Figure S1 in Supporting Information), which indicated that it would be the optimal

observation time for skeletal system imaging of the nude mouse. After 168 h, fluorescence signals could not be detected from structures of the skeletal system any more, while metabolic organs such as the liver and the spleen still showed weak fluorescence signals (Fig. 1h).

Figure 1. (a) Photograph of Balb/C nude mouse. (b-i) Real-time SWIR fluorescence imaging of Balb/C nude mouse by RNase A-PbS QDs (posterior view) with images acquired at 5 min, 15 min, 30 min, 60 min, 4 h, 24 h, 72 h and 168 h post-injection, respectively. (i) X-ray photo and (j) SWIR image of bones in an overall view (prone position). (k) X-ray photo and (l) SWIR image of bones in an overall view (supine position). (m-q) Zoomed images of (i-l) respectively. (r) SWIR image of the skull.

Notably, from posterior view, as shown Figure S2 in Supporting Information, FL intensity in both the skull and the spine was higher than that in the other structures of the skeletal system at 1 h post-injection, which showed both the skull and the spine has a superior imaging among other observed bone structures from a posterior view. this phenomenon is ascribed to the anatomical and structural characteristics around the skull and the spine (Figure S2b in Supporting Information). Anatomically, both of the two bone structures had a relatively abundant source of blood flow from the carotid artery, aorta and common iliac artery, while an extraordinarily large vascularity named Adamkiewicz artery from the thoracolumbar segment provided mostly blood supply for the spinal cord[22, 23]. On the other hand, as the vertebral vein had no valve, the blood could flow in both directions[22], increasing the dwelling time of QDs and facilitating high FL intensity of the spine. Interestingly, from anterior view (Figure S3 in Supporting Information), although similar results of imaging were obtained comparable to the posterior view, the lower extremities were imaged quicker than the upper extremities, due to the fact that the anterior side of the lower extremities was covered by fewer muscles than the posterior side. Furthermore, those *in vivo* imaging evaluations were also repeated in the Balb/C mouse in order to confirm the above results. No obvious differences between the Balb/C mouse and the Balb/C nude mouse were observed in SWIR imaging (Figure S4, S5 and Movie S3, S4 in Supporting Information).

To investigate the features of *in vivo* SWIR fluorescence imaging, a comparison with X-ray imaging was made and shown in Fig. 1i-r. From a posterior view (prone position), the pelvis overlapped with other structures and could not be fully recognized under X-ray examination (Fig. 1i and Fig. 1n). Compared with X-ray imaging, morphology of the pelvis could be clearly distinguished with a full shape of both the ilium and the sacrum in SWIR fluorescence imaging (Fig. 1j and Fig. 1o). While from an anterior view (supine position), the sternum could be recognized and differentiated as a segmental structure, which integrated with the background under X-ray imaging (Fig. 1k, l, p and q). Notably, regarding the skull, both the left and right lateral ventricles could be observed from the SWIR images, which could not be distinguished with X-ray images (Fig. 1m and Fig. 1r). Unlike traditionally two-dimensional anatomical structures under X-ray (Fig. 1i and Fig. 1k), our QDs-based SWIR fluorescence imaging was capable of generating highly-magnified and well-resolved images for frequent and longitudinal studies of bones without radiation in the future.

Most importantly, as shown in Fig. 1m and Fig. 1r, both the maxillary and the parietal of the skull have much clearer and more stratified morphology than that in X-ray images. The result showed that the substructure and biological activities of the skull could be analyzed by QDs-based SWIR imaging. Interestingly, simultaneous with bone imaging, the contours of the liver, spleen and heart could only be clearly demonstrated by SWIR, not by X-ray. The additional information exhibited by SWIR imaging had great potential to offer a comprehensive diagnosis of organs injuries accompanied with acute trauma, especially for the organs with abundant blood supply or neighboring fracture zones. Therefore, compared with X-ray imaging, RNase A-PbS QDs-guided SWIR *in vivo* imaging not only demonstrated a multi-spatial resolution imaging of the skeletal system based on tissue penetration and viewing angle without radiation exposure, but also provided a precise overall risk evaluation for bone disorders, especially for trauma in clinical practice.

To further confirm the *in vivo* results above, *ex vivo* imaging of the isolated bone tissues of both Balb/C nude mouse and Balb/C mouse after QDs injection was obtained following *in vivo* observation (Fig. 2). Comparable with the *in vivo* results, the FL intensity was obviously higher in the skull, the spine and four limbs than other bone structures due to blood supply. However, as shown in Fig. 2a and Fig. 2b, the FL intensity of bone structures quickly decreased from 3 h to 72 h in both Balb/C nude mouse and Balb/C mouse. It was much quicker than that in *in vivo* imaging observation, because the fluorescence of bone structures could preserve for 168 hours in *in vivo* imaging. The quick fading of fluorescence detected in the isolated bone tissues was probably due to the exposure of QDs with various factors such as surface ligands, pH value of the solvent, photooxidation in the environment and so on[24]. Moreover, after tissue isolation from the living body, cells died over time *in vitro*, leading to decomposition of QDs accompanied with a rapid decrease of FL intensity[25, 26]. Therefore, the binding capability of RNase A-PbS QDs could depend on cell states including living cells and died cells, providing extra information about the biological activities of bone tissues.

As the fluorescence of bone structures could be partially interfered with soft tissues, the skeletal structures were isolated and examined by SWIR fluorescence imaging and X-ray imaging *ex vivo*. As shown in Fig. 2c-j, strong fluorescence signals were detected from the sternum (Fig. 2g and Fig. 2i, green arrow), the ribs (Fig. 2i, white arrow) and the lumber vertebrae (Fig. 2h and Fig. 2j), which agreed with previous SWIR *in vivo* imaging. Particularly, Figure S6 in Supporting Information demonstrated the segmented bone structures of rib and sternum in details with the SWIR images, while it was not visualized under X-ray. Moreover, these small bone pieces with a diameter less than 0.1 cm in the sternum could be clearly identified in SWIR images and X-ray images. This result suggested that SWIR imaging would be an alternative approach of X-ray for bone microstructure in future. Therefore, SWIR imaging would provide a dynamic monitoring for both physiological and pathological processes of bone, benefiting for the diagnosis of skeletal disease in future.

As shown in Fig. 3a, to further study the underlying mechanism of SWIR QDs-guided bone imaging, four cell types related with bone metabolism including osteoblasts (MC3T3-E1), fibroblasts (NIH3T3), BMSC and Macrophages (RAW264.7) were selected[27–31]. It was reported that QDs could non-specifically bind

with cell membranes before entering cells[32–35], In this work, the cells were rinsed by PBS twice to remove those non-specifically QDs bound to cell membranes. As shown in Fig. 3b, fluorescence signals were detected in the four types of cells after 0.5 h, 3 h, 24 h and 48 h of incubation. Among the four, the FL intensity of MC3T3-E1 cells reached a peak after three hours of incubation, which suggested that MC3T3-E1 cells were more easily to uptake QDs than the other three cells types (NIH3T3, BMSCs and RAW264.7). Moreover, similar results were also detected from those four cell types before rinsing (Figure S7 in Supporting Information). Moreover, the FL intensity reached a peak when the QDs concentration was around 250 μg mL^{-1} (Figure S8 in Supporting Information), and the MC3T3-E1 cells still showed the highest FL intensity in comparison with the other tested cell types at the same concentration, which further proved the unique binding relationship between QDs and MC3T3-E1 cells.

To further study the relationship between QDs and the cell lifecycle, these QDs used in the first round of cell culture were collected and recycled as a medium additive for the second round of cell culture). Surprisingly, no fluorescence signals were detected after 48 hours of incubation, suggesting that only freshly prepared QDs was able to maintain its fluorescence in the first round of cell incubation, while second-hand QDs could lose fluorescence after cell metabolism in the second round of cell incubation. Therefore, as shown in Fig. 3a, the QDs' fluorescence could be quenched after cell metabolism and would eventually be eliminated from the body without disturbing SWIR imaging in the next time.

Although *in vivo* results revealed that QDs in bone tissues were eliminated up to 80% after 72 hours, while most were cleared out from internal organs (such as the liver and the spleen) after 168 hours. Therefore, as shown in Fig. 3c and Figure S9 in Supporting Information, bone tissues and main organs in the tested mouse showed no obvious inflammation and abnormality after QDs injection, indicating our prepared QDs had excellent biocompatibility, in agreement with our previous studies[36, 37].

Conclusion

In summary, we successfully achieved a super-resolution SWIR imaging of bone structures *in vivo* and *ex vivo* by using RNase A-PbS QDs as a bone specific imaging contract, indicating SWIR *in vivo* imaging based on RNase A-PbS QDs would serve as a novel imaging approach for bone research. More importantly, 1 h post-injection was considered the optimal time for *in vivo* observation and imaging for mice in this work, which facilitated optimization the time of bone imaging in human. Particularly, owing to blood supply and peripheral circulation near bones, both the skull and the spine had a superior resolution imaging over the other bone structures, making them more suitable for SWIR *in vivo* imaging. Besides,SWIR *in vivo* imaging could also reveal the biological activities of the bones and the inter organs after QDs injection, indicating that our *in vivo* SWIR imaging could provide a live imaging of the skeletal system. Notably, the underlying mechanism of SWIR imaging for bone might be ascribed to the highly-specific binding between RNase A-PbS QDs and MC3T3-E1 cells rather than NIH3T3, BMSC and RAW264.7 cells. In a word, SWIR *in vivo* imaging based on RNase A-PbS QDs, by removing the barriers of radioactive imaging, is not only a cutting-edge technology for the fundamental understanding of bone, but also serves as a promising imaging tool for diagnosis of skeletal diseases in clinical practice.

Declarations

Experimental Section

Find in the supporting information.

Supporting Information

Supporting Information is available from the authors.

Corresponding Author

Email zcheng@stanford.edu (Prof. Zhen Cheng)

Email zongping_luo@yahoo.com (Prof. Zongping Luo)

Email biochenjun@fudan.edu.cn (Prof. Jun Chen)

Acknowledgements

Y. Che, S. Feng and J. Guo contributed equally to this work. This work was supported by National Natural Science Foundation of China (No. 81572108, No.81972129, No. 81772339, and No. 31570943), The Key Clinical Medicine Center of Shanghai (2017ZZ01006), Sanming Project of Medicine in Shenzhen (SZSM201612078), Shanghai Rising-Star Project (18QB1400500), The Introduction Project of Clinical Medicine Expert Team for Suzhou (SZYJTD201714), The Priority Academic Program Development of Jiangsu Higher Education Institutions, Shanxi provincial Health Commission Project (2018124), Science and Technology Innovation Project of Shanxi Higher Education (2019L0690), Development Project of Shanghai Peak Disciplines-Integrative Medicine (20180101) and Shanghai Committee of Science and Technology (19441901600 and 19441902000).

Ethics

This work received the approval of Ethics by Ethics Committee of Soochow University (ECSU-201700035).

Consents for publication

Consents for publication were received from all authors.

Competing interests

The authors showed no competing interests.

References

1. Datta HK, Ng WF, Walker JA, Tuck SP, Varanasi SS. The cell biology of bone metabolism. J Clin Pathol. 2008;61:577–87.
2. Johnston CC Jr, Slemenda CW, Melton LJ 3. Clinical use of bone densitometry. N Engl J Med. 1991;324:1105–9. rd. ; .
3. Orlic D, Kajstura J, Chimenti S, Jakoniuk I, Anderson SM, Li B, et al. Bone marrow cells regenerate infarcted myocardium. Nature. 2001;410:701–5.
4. Grüneboom A, Kling L, Christiansen S, Mill L, Maier A, Engelke K, et al. Next-generation imaging of the skeletal system and its blood supply. Nat Rev Rheumatol. 2019;15:533–49.
5. Andrews JC, Brennan S, Patty C, Luening K, Pianetta P, Almeida E, et al. A High Resolution, Hard X-ray Bio-imaging Facility at SSRL. Synchrotron Radiation News. 2008;21:17–26.
6. Rao J, Dragulescu-Andrasi A, Yao H. Fluorescence imaging in vivo: recent advances. Curr Opin Biotechnol. 2007;18:17–25.
7. Hilderbrand SA, Weissleder R. Near-infrared fluorescence: application to in vivo molecular imaging. Curr Opin Chem Biol. 2010;14:71–9.
8. Moerner WE, Fromm DP. Methods of single-molecule fluorescence spectroscopy and microscopy. 2003; 74: 3597–619.
9. Juette MF, Terry DS, Wasserman MR, Zhou Z, Altman RB, Zheng Q, et al. The bright future of single-molecule fluorescence imaging. Curr Opin Chem Biol. 2014;20:103–11.
10. Hong G, Lee JC, Robinson JT, Raaz U, Xie L, Huang NF, et al. Multifunctional in vivo vascular imaging using near-infrared II fluorescence. Nat Med. 2012;18:1841–6.
11. Fan Y, Wang P, Lu Y, Wang R, Zhou L, Zheng X, et al. Lifetime-engineered NIR-II nanoparticles unlock multiplexed in vivo imaging. Nat Nanotechnol. 2018;13:941–6.
12. Hong G, Diao S, Chang J, Antaris AL, Chen C, Zhang B, et al. Through-skull fluorescence imaging of the brain in a new near-infrared window. Nat Photonics. 2014;8:723–30.
13. Yang Y, Chen J, Shang X, Feng Z, Chen C, Lu J, et al. Visualizing the Fate of Intra-Articular Injected Mesenchymal Stem Cells In Vivo in the Second Near-Infrared Window for the Effective Treatment of Supraspinatus Tendon Tears. Adv Sci (Weinh). 2019;6:1901018.
14. Xu H, Chen J, Feng Z, Fu K, Qiao Y, Zhang Z, et al. Shortwave infrared fluorescence in vivo imaging of nerves for minimizing the risk of intraoperative nerve injury. Nanoscale. 2019;11:19736–41.
15. Chen J, Kong Y, Wang W, Fang H, Wo Y, Zhou D, et al. Recycled synthesis of Whey-Protein-Capped lead sulfide quantum dots as the second near-infrared reporter for bioimaging application. ACS Sustainable Chemistry Engineering. 2016;4:2932–8.
16. He S, Chen S, Li D, Wu Y, Zhang X, Liu J, et al. High Affinity to Skeleton Rare Earth Doped Nanoparticles for Near-Infrared II Imaging. Nano Lett. 2019;19:2985–92.
17. Hong G, Antaris AL, Dai H. Near-infrared fluorophores for biomedical imaging. Nature Biomedical Engineering. 2017;1:0010.

18. Wang F, Wan H, Ma Z, Zhong Y, Sun Q, Tian Y, et al. Light-sheet microscopy in the near-infrared II window. Nat Methods. 2019;16:545–52.
19. Wan H, Du H, Wang F, Dai H. Molecular Imaging in the Second Near-Infrared Window. 2019; 29: 1900566.
20. Hu Z, Fang C, Li B, Zhang Z, Cao C, Cai M, et al. First-in-human liver-tumour surgery guided by multispectral fluorescence imaging in the visible and near-infrared-I/II windows. Nature Biomedical Engineering. 2019.
21. Kong Y, Chen J, Fang H, Heath G, Wo Y, Wang W, et al. Highly Fluorescent Ribonuclease-A-Encapsulated Lead Sulfide Quantum Dots for Ultrasensitive Fluorescence in Vivo Imaging in the Second Near-Infrared Window. Chem Mater. 2016;28:3041–50.
22. Panjabi MM, Goel V, Oxland T, Takata K, Duranceau J, Krag M, et al. Human lumbar vertebrae. Quantitative three-dimensional anatomy. Spine (Phila Pa 1976). 1992;17:299–306.
23. Vollmer DG, Banister WM. Thoracolumbar spinal anatomy. Neurosurg Clin N Am. 1997;8:443–53.
24. Fischer HC, Liu L, Pang KS, Chan WCW. Pharmacokinetics of Nanoscale Quantum Dots: In Vivo Distribution, Sequestration, and Clearance in the Rat. AFM. 2006;16:1299–305.
25. Akerman ME, Chan WC, Laakkonen P, Bhatia SN, Ruoslahti E. Nanocrystal targeting in vivo. Proc Natl Acad Sci U S A. 2002;99:12617–21.
26. Gao X, Cui Y, Levenson RM, Chung LW, Nie S. In vivo cancer targeting and imaging with semiconductor quantum dots. Nat Biotechnol. 2004;22:969–76.
27. Gow DJ, Sauter KA, Pridans C, Moffat L, Sehgal A, Stutchfield BM, et al. Characterisation of a novel Fc conjugate of macrophage colony-stimulating factor. Mol Ther. 2014;22:1580–92.
28. Lloyd SA, Yuan YY, Simske SJ, Riffle SE, Ferguson VL, Bateman TA. Administration of high-dose macrophage colony-stimulating factor increases bone turnover and trabecular volume fraction. J Bone Miner Metab. 2009;27:546–54.
29. Vi L, Baht GS, Whetstone H, Ng A, Wei Q, Poon R, et al. Macrophages promote osteoblastic differentiation in-vivo: implications in fracture repair and bone homeostasis. J Bone Miner Res. 2015;30:1090–102.
30. Galicka A, Surazynski A, Wolczynski S, Palka J, Popko J, Gindzienski A. Phenotype variability in a daughter and father with mild osteogenesis imperfecta correlated with collagen and prolidase levels in cultured skin fibroblasts. Ann Clin Biochem. 2005;42:80–4.
31. Locklin RM, Williamson MC, Beresford JN, Triffitt JT, Owen ME. In vitro effects of growth factors and dexamethasone on rat marrow stromal cells. Clin Orthop Relat Res. 1995: 27–35.
32. Jaiswal JK, Mattoussi H, Mauro JM, Simon SM. Long-term multiple color imaging of live cells using quantum dot bioconjugates. Nat Biotechnol. 2003;21:47–51.
33. Voura EB, Jaiswal JK, Mattoussi H, Simon SM. Tracking metastatic tumor cell extravasation with quantum dot nanocrystals and fluorescence emission-scanning microscopy. Nat Med. 2004;10:993–8.

34. Kloepfer JA, Mielke RE, Nadeau JL. Uptake of CdSe and CdSe/ZnS quantum dots into bacteria via purine-dependent mechanisms. Appl Environ Microbiol. 2005;71:2548–57.
35. Chen F, Gerion D. Fluorescent CdSe/ZnS Nanocrystal-Peptide Conjugates for Long-term, Nontoxic Imaging and Nuclear Targeting in Living Cells Nano Letters. 2004; 4: 1827–32.
36. Chen J, Kong Y, Wang W, Fang H, Wo Y, Zhou D, et al. Direct water-phase synthesis of lead sulfide quantum dots encapsulated by beta-lactoglobulin for in vivo second near infrared window imaging with reduced toxicity. Chem Commun (Camb). 2016;52:4025–8.
37. Kong Y, Chen J, Gao F, Brydson R, Johnson B, Heath G, et al. Near-infrared fluorescent ribonuclease-A-encapsulated gold nanoclusters: preparation, characterization, cancer targeting and imaging. Nanoscale. 2013;5:1009–17.
38. Feng S, Chen J, Wo Y, Li Y, Chen S, Zhang Y, et al. Real-time and long-time in vivo imaging in the shortwave infrared window of perforator vessels for more precise evaluation of flap perfusion. Biomaterials. 2016;103:256–64.

Figures

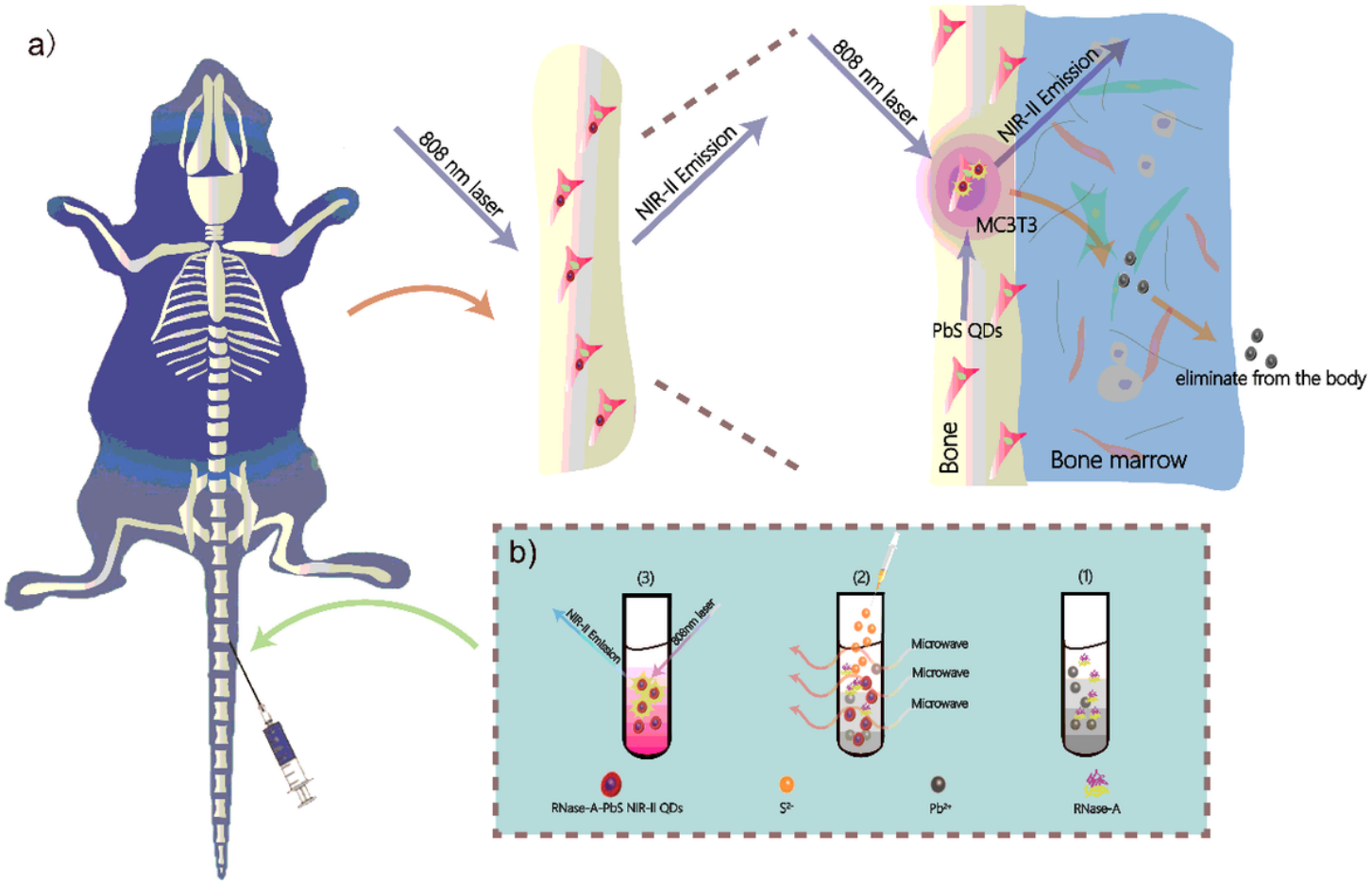

Figure 1

(a) Schematic diagram of the dynamic evaluation of bone based on RNase A-PbS QDs-guided fluorescence imaging at the SWIR window. (b) Schematic illustration of the synthesis of the RNase A-PbS QDs.

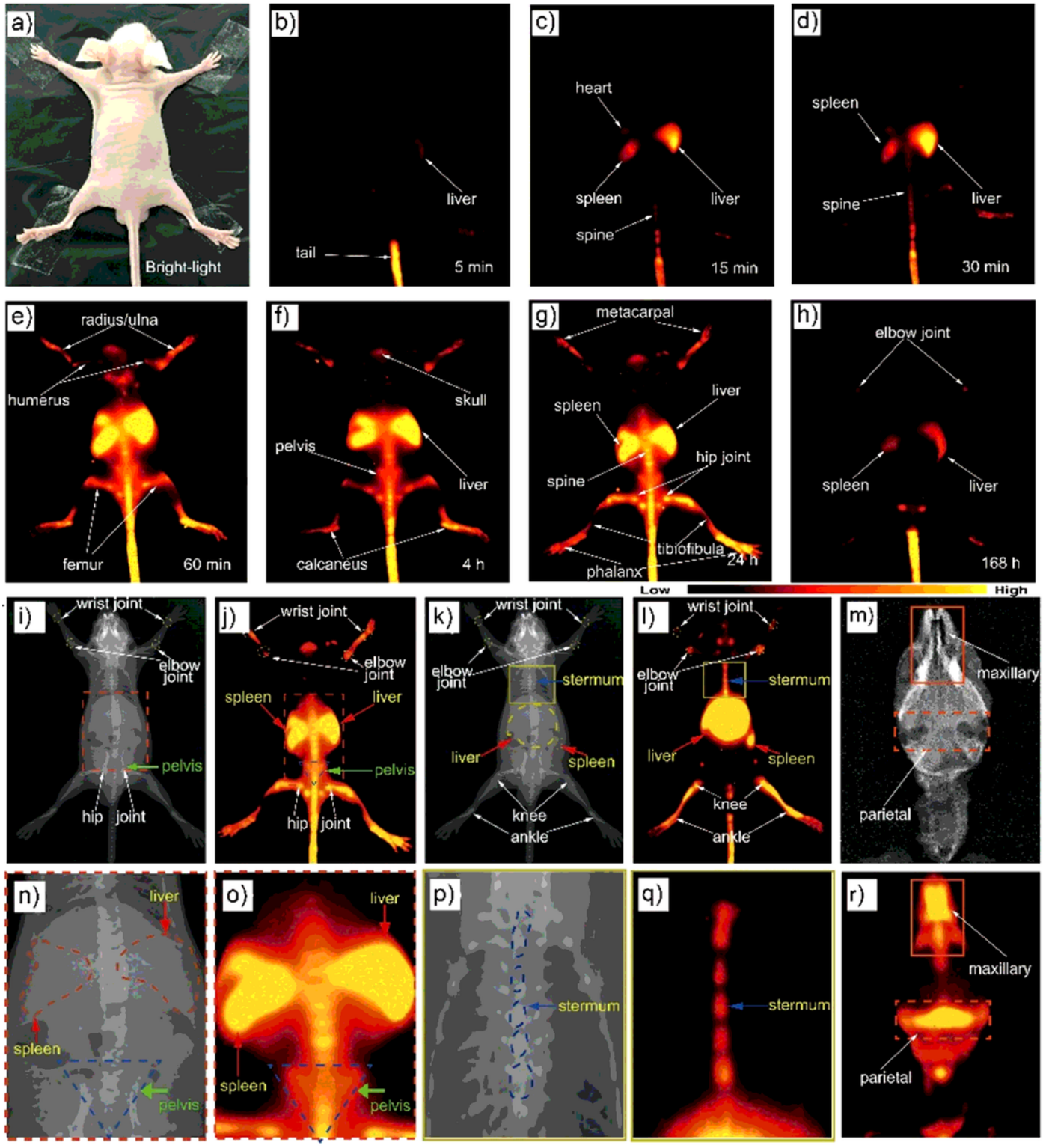

Figure 2

(a) Photograph of Balb/C nude mouse. (b-i) Real-time SWIR fluorescence imaging of Balb/C nude mouse by RNase A-PbS QDs (posterior view) with images acquired at 5 min, 15 min, 30 min, 60 min, 4 h, 24 h, 72

h and 168 h post-injection, respectively. (i) X-ray photo and (j) SWIR image of bones in an overall view (prone position). (k) X-ray photo and (l) SWIR image of bones in an overall view (supine position). (m-q) Zoomed images of (i-l) respectively. (r) SWIR image of the skull.

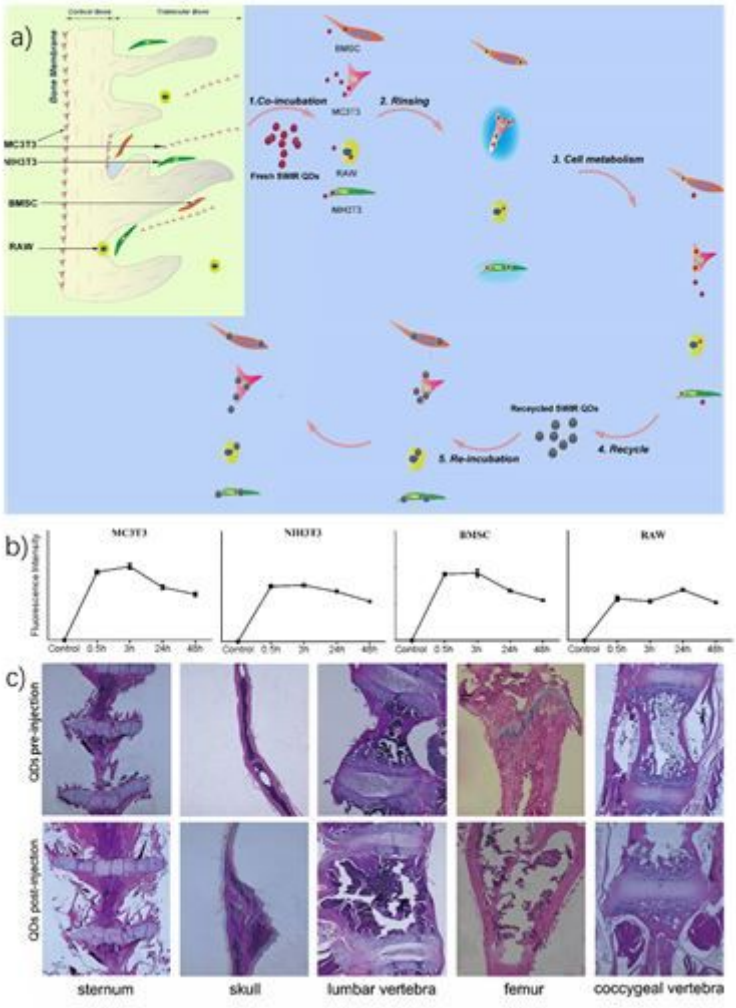

Figure 3

(a) Schematic of cell imaging based on RNase A-PbS QDs-guided real-time imaging at the SWIR window. (b) Statistical analysis of the variation of QDs fluorescence intensity regarding the concentration of QDs solution. (c) Histological analysis of typical bone tissues before and after QDs injection 168 h.

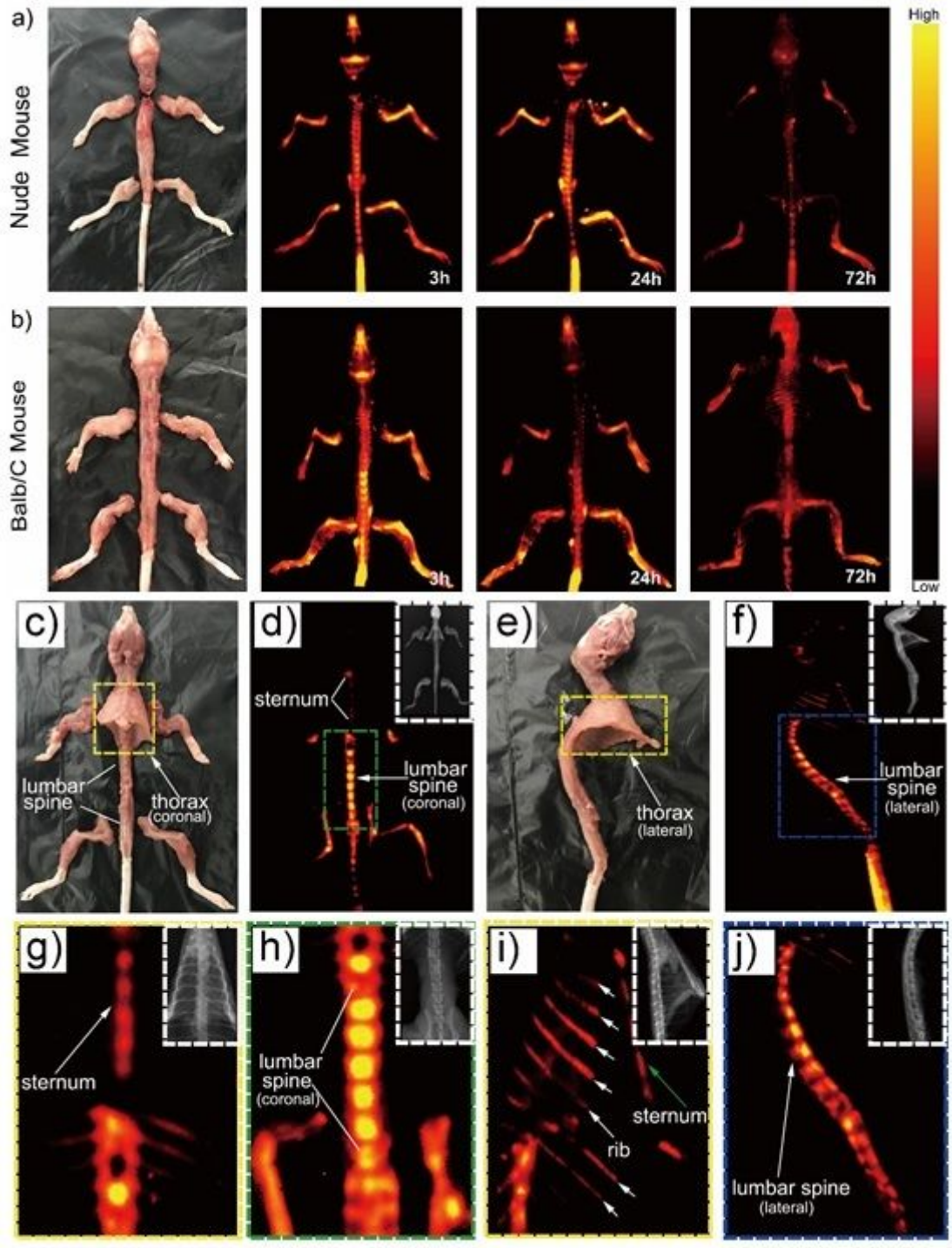

Figure 4

Ex vivo SWIR imaging of the isolated bone tissues of (a) Balb/C nude mouse and (b) Balb/C mouse. (c) (e) Bright-light photos of bone tissues. (d) (f) SWIR images of ex vivo bone tissues. (g-j) Zoomed SWIR images of (d) and (f).

Supplementary Files

This is a list of supplementary files associated with this preprint. Click to download.

- MS4.mp4
- MS3.mp4
- MS2.mp4
- MS1.mp4
- SupportingInformationnanobio.docx